Progress In Electromagnetics Research M, Vol. 90, 167–184, 2020

Printed 5G MIMO Antenna Arrays in Smartphone Handset for LTE Bands 42/43/46 Applications

Haneen S. Aziz and Dhirgham K. Naji*

Abstract—In this paper, a dual-band 4-, 6-, and 8-element multiple-input multiple-output (MIMO) antenna arrays operating at the sub-6-GHz (LTE 42/43 and 46) bands for the fifth-generation (5G) smartphones are proposed. To realize these three MIMO applications in two LTE bands, miniaturized spiral and meander line-shaped strips coupled-fed patch antenna elements are printed on the front side of an FR4 system circuit board and are able to excite two resonance modes. Polarization and spatial diversity techniques are applied to these elements so that the enhanced isolation and reduced coupling effects can be attained. The proposed single antenna element besides 8-element antenna array has been fabricated and experimentally measured. Desirable simulated and measured S-parameters (reflection and transmission coefficients) are obtained for the antenna arrays over the working dual frequency bands. The diversity performance, such as the envelope correlation coefficient (ECC) and diversity gain (DG), has also been simulated and analyzed. Moreover, the performance results, antenna gain, and efficiency over the bands and radiation patterns at the specified resonant frequencies are also presented.

1. INTRODUCTION

Due to the increased demand of mobile communication system for overcoming some unwanted phenomena such as multipath fading, large latency, and low data-rate transmission, the fifth generation (5G) system is considered as a promising solution over the current 4G (fourth generation) system [1–3]. To improve both the link reliability and channel capacity or spectrum efficiency in the 5G environment, a well-known antenna diversity technique is usually demonstrated in the available literature by using multiple-input and multiple-output (MIMO) antenna systems. Despite the above-mentioned positive aspects of a MIMO system, there are still many challenges for researchers in designing a compact multi-antenna system for mobile devices having better antenna performance in terms of low mutual coupling and envelope correlation coefficient (ECC) between the antenna elements [4]. In future 5G system below sub-6 GHz spectrum, long term evolution (LTE) communication bands LTE 42/43 (3400–3600 MHz/3600–3800 MHz) and LTE 46 (5150–5925 MHz) besides LTE 2300 (2300–2400 MHz) and LTE 2500 (2540–2620 MHz) have been adopted as standards for smartphones with a massive MIMO antenna array [5–13]. In a massive MIMO scheme, a relative large number of compact LTE antennas ($N \geq 6$ or 8) arranged at the two sides of a mobile printed circuit board (PCB) with high antenna efficiency and low ECC should be adopted for operation in a 5G communication system [14]. To increase the number of antennas within a limited space while maintaining the main requirements of the aforementioned 5G, maximization in diversity gain and improvement of the isolation between closely miniature antenna elements have become a persistent need in the future for MIMO antenna designs. Furthermore, the increasing demand of massive MIMO systems for multiband and multimode applications suitable for

Received 19 January 2020, Accepted 5 March 2020, Scheduled 19 March 2020

* Corresponding author: Dhirgham K. Naji (dhrgham.kamal@gmail.com).

The authors are with the Department of Electronic and Communications Engineering, College of Engineering, Al-Nahrain University, Baghdad, Iraq.

the aforementioned LTE bands in 5G smartphones encourages different antenna research groups to pay deep attention to solve the associated challenges and limitations.

In recent years, many techniques and methods have been reported for 5G MIMO antenna array in smartphone handsets operating at the sub-6 GHz spectrum [15–17]. These MIMO system designs are single resonance mode (or operating in single band) antenna structures and lack LTE 46 band. To obtain an impedance bandwidth that can cover both the LTE 42 and/or LTE 43 and LTE 46 bands, several 5G MIMO antenna designs have been reported in the last few years. In these papers, different techniques have successfully demonstrated 5G arrays with 8 or 10 antenna elements aiding reduction of mutual coupling and dual-band operation, such as a T-shaped coupled-fed slot antenna array [5], a stepped impedance resonator (SIR) [18], and a protruded parasitic structure etched on the ground plane [19]. However, although the previously reported works have provided antenna arrays in multiband below 6 GHz for 5G smartphone applications, it is still difficult for antenna engineers to design a compact 5G MIMO antenna array having multi-modes and multi-bands, which offers good MIMO performance and radiation characteristics

Therefore, in this paper, multiband and dual-mode 4-, 6-, and 8-antenna array designs for 5G smartphone applications are proposed. Due to their interesting features for size miniaturization and multiband characteristics, the meander-line- and spiral-shaped geometries [20–22] are widely used for antenna designs. These geometries are used for each array element, which is composed of a single-turn spiral structure and meander line-shaped strip, and its low and high bands are able to cover LTE bands 42/43 (3.4–3.8 GHz) and LTE band 46 (5.150–5.925 GHz), respectively. This antenna element is successfully designed to cover the aforementioned bands with a miniaturized dimension of 11 mm × 14 mm, and an acceptable performance has been obtained. Based on the designed single antenna element, three antenna arrays integrate 4, 6, and 8 isolated MIMO antennas arranged in orthogonal manner, and are wide enough to enhance 5G MIMO in most sub-6 GHz bands. Polarization diversity is obtained, and thanks to good isolation, pattern diversity is also achieved. The proposed single antenna element and three MIMO antenna arrays are simulated by using the electromagnetic software tool (CST Microwave Studio), and their performance results in terms of S-parameters (reflection and transmission coefficients), antenna gains and efficiencies besides radiation patterns are shown. Then, in order to verify the MIMO performances, envelope correlation coefficient (ECC) and diversity gain (DG) are also computed. Lastly, prototypes of the single antenna and 8-antenna array are fabricated and measured, and an acceptable agreement between simulated and measured results is achieved.

2. DESIGN, ANALYSIS AND PERFORMANCE OF SINGLE ANTENNA ELEMENT

2.1. Antenna Configuration

The layout configuration of the proposed single antenna element is shown in Fig. 1. As can be noticed, the radiating patch composed of the combinations of a single-turn spiral structure and two sections of meander line-shaped geometry is printed on the front side of an FR-4 substrate (height $h_{sub} = 0.8$ mm,

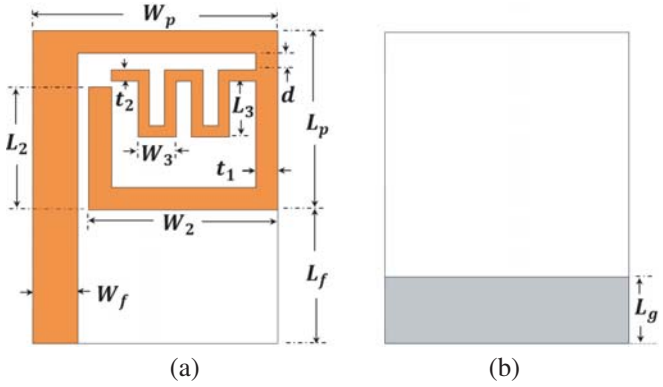

Figure 1. Layout of the proposed monopole antenna. (a) Front view. (b) Back view.

relative permittivity $\epsilon_r = 4.3$, and tangent loss $\tan\delta = 0.025$), and on the back side of substrate a partial ground of length ($L_g = 3\,\text{mm}$) is used. The optimized dimensions of the proposed antenna are: patch length ($L_p = 8\,\text{mm}$), patch width ($W_p = 11\,\text{mm}$), thickness ($t_1 = 1\,\text{mm}$), spiral length and width ($L_2 = 5.5\,\text{mm}$) and ($W_2 = 8.5\,\text{mm}$), respectively, and meander line is characterized by the parameters: vertical and horizontal lengths ($L_3 = 2.5\text{mm}$) and ($W_3 = 1.7\,\text{mm}$) respectively, thickness ($t_2 = 0.5\,\text{mm}$), and the distance ($d = 1\,\text{mm}$) over which the mender line is inscribed within the spiral structure. A stripline-fed rectangular structure having characteristic impedance of $50\,\Omega$ with length ($L_f = 8\,\text{mm}$) and width ($W_f = 2\,\text{mm}$) is used for feeding antenna through a miniature-A (SMA) connector. A CST Microwave Studio (MWS) is employed for extensive simulations, parametric analysis, and performance evaluation of the proposed antenna.

2.2. Evolution Design Steps and the Working Principle of the Single Antenna

Six evolution design steps besides the working principle are introduced herein to analyze the performance of the proposed single antenna element. Fig. 2 shows these design steps, and their geometric parameters are listed in Table 1. The magnitude of reflection coefficient $|S_{11}|$ curves are plotted in Fig. 3. These six design steps are discussed, and their performance are described in detail as follows:

Step 1 (Ant0): In the first step, an inset-fed rectangular microstrip antenna (RMSA), as shown in Fig. 2(a), is designed by assuming that the specified information includes the resonant frequency

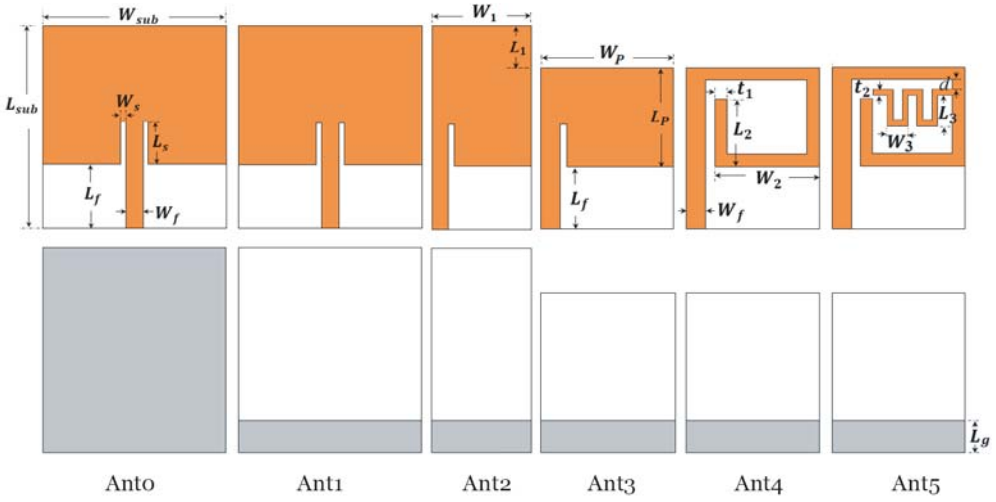

Figure 2. Six prototypes of the proposed single antenna, front view (in the upper part), back view (in the lower part).

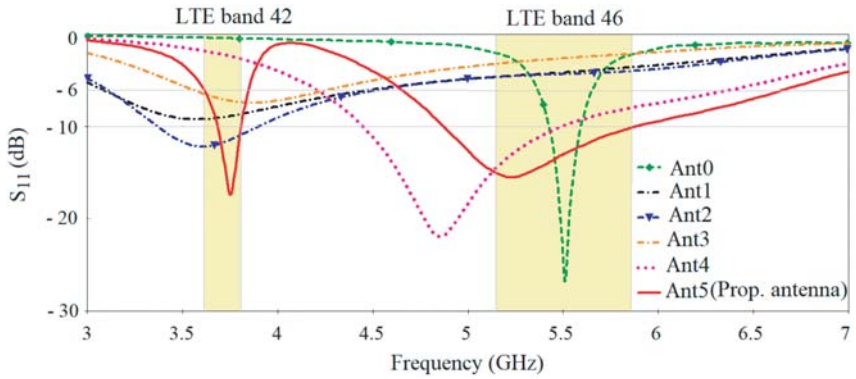

Figure 3. Simulated input reflection coefficient (S_{11}) for antennas (Ant0–Ant5).

Table 1. The dimensions of the proposed six antennas.

Parameter	Value (mm)					
	Ant0	**Ant1**	**Ant2**	**Ant3**	**Ant4**	**Ant5**
L_{sub}	19.3	-	-	-	-	-
W_{sub}	17.3	-	-	-	-	-
h_{sub}	0.8	0.8	0.8	0.8	0.8	0.8
L_s	4.2	4.2	4.2	4.2	-	-
W_s	0.5	0.5	0.5	0.5	-	-
L_f	6.0	6.0	6.0	6.0	6.0	6.0
W_f	2.0	2.0	2.0	2.0	2.0	2.0
L_1	-	-	5.3	-	-	-
W_1	-	-	9.65	-	-	-
L_p	-	-	-	8.0	8.0	8.0
W_p	-	-	-	11.0	11.0	11.0
L_2	-	-	-	-	-	5.5
W_2	-	-	-	-	-	8.5
L_3	-	-	-	-	-	2.5
W_3	-	-	-	-	-	1.7
t_1	-	-	-	-	-	1.0
t_2	-	-	-	-	-	0.5
d	-	-	-	-	-	1.0
L_g	-	3.0	3.0	3.0	3.0	3.0

f_r, dielectric constant ε_r, and the height of substrate h_{sub}. By substituting these specified parameters as: $f_r = 5.5\,\text{GHz}$, $\varepsilon_r = 4.3$, and $h_{sub} = 0.8\,\text{mm}$ in the transmission line model [23], one can get the patch dimensions as $W_p = 16.75\,\text{mm}$ and $L_p = 12.40\,\text{mm}$. As shown in Fig. 2(a) and Table 1 for the optimized Ant0, which is designed through a CST MWS, the total substrate dimensions, $L_{sub} \times W_{sub}$, are 19.3mm $\times$ 17.3 mm, and the patch width and length $W_p = W_{sub} = 16.75\,\text{mm}$ and $L_p = L_{sub} - L_f = 11.3\,\text{mm}$, respectively. It is observed from Fig. 3 that Ant0 covers single frequency band with resonant frequency of 5.5 GHz. Hence, Ant0 represents the reference antenna covering the desired upper frequency band (LTE 46) from which the miniaturized proposed antenna is designed to cover both the lower and upper frequency bands (LTE 43/46) for 5G applications.

Step 2 (Ant1): In the second design step, Ant1 is achieved after setting the length of ground plane $L_g = 3\,\text{mm}$ instead of $L_g = L_{sub} = 19.3\,\text{mm}$ used for Ant0, and this value of L_g remains the same for all the succeeding designed antennas (Ant2–Ant5). As seen in Fig. 3, Ant1 resonates at 3.57 GHz with $|S_{11}| = -9.2\,\text{dB}$, meaning that the $-10\,\text{dB}$ impedance bandwidth (BW) is zero.

Step 3 (Ant2): In order to miniaturize the size of proposed antenna, the left half part of Ant1 is removed since the electric field or voltage is nearly equal to zero at centre of the antenna. As a result, Ant2 is produced with total dimensions of $L_{sub} \times W_1$ being $19.3\,\text{mm} \times 9.65\,\text{mm}$ and $W_1 = 0.5W_{sub} + 0.5W_f = 9.65\,\text{mm}$. Ant2 enhances the $-10\,\text{dB}$ impedance BW to be 530 MHz ranging from 3.37 to 3.90 GHz at resonance frequency of 3.6 GHz (see Fig. 3). Thus, Ant2 represents the main antenna from which the proposed antenna is achieved.

Step 4 (Ant3): In this step, Ant3 is evolved from Ant2 by reducing its substrate length by L_1 and slightly increasing its substrate width to be $W_p = 11\,\text{mm}$ instead of 9.65 mm, which means that the total dimension of Ant3 is $(L_p + L_f) \times W_p = 14\,\text{mm} \times 11\,\text{mm}$. As observed from Fig. 2, Ant3 represents the zero iteration of spiral structure while maintaining the same overall dimension value of $14\,\text{mm} \times 11\,\text{mm}$ for the remaining two antennas (Ant4 and Ant5) that will be subsequently designed in steps 5 and 6. It is seen from Fig. 3 that Ant3 operates at 3.87 GHz with $|S_{11}| = -7.42\,\text{dB}$, and as stated before a

modification in Ant3 is needed to attain an antenna having the desired dual-band response.

Step 5 (Ant4): In the fifth step, Ant4 is the first iteration of spiral structure with total dimensions similar to that of Ant3. A spiral strip of thickness t_1, the outer length and width L_p and $W_p - W_f$, and the inner length and width L_2 and W_2, respectively is connected to a 50 Ω strip line. As shown in Fig. 3, the impedance BW of Ant4 is enhanced at about 1.05 GHz ranging from 4.45 to 5.50 GHz with a resonance frequency of 4.85 GHz. It is noted that all the previous antennas having a single band characteristic, and thus it is needed to modify or add resonant structure to Ant4 for covering the desired dual-band response.

Step 6 (Ant5): In this sixth and final step of the design procedure, a meander line with two sections of length and width L_3 and W_3, respectively and thickness t_2 is placed at distance d from the upper part of the spiral structure [see Ant5 in Fig. 2]. It is observed from Fig. 3 and Table 2 that Ant5 operates at two resonance frequencies covering the LTE 43/46 bands for −6 dB BW criterion.

Table 2. The final frequency bands (in GHz) of the proposed designed antenna.

Frequency bands	**Lower Band**		**Upper frequency**	
Criterion	**−6 dB**	**−10 dB**	**−6 dB**	**−10 dB**
LTE 43	3.61	3.68	3.84	3.80
LTE 46	4.65	4.87	6.66	5.87

In order to further understand the working principle of the single antenna design, the impact of the basic geometric parameters L_3, W_3, L_p, and L_g on the antenna performance of S_{11} curve is studied. These optimized parameters used for designing the proposed antenna, as (in red) for S_{11} curves in Figs. 4(a)–(d), respectively are: $L_3 = 2.5$ mm, $W_3 = 1.7$ mm, $L_p = 8$ mm, and $L_g = 3$ mm. The other parameters maintain their values as in Table 1 during studying the aforementioned basic parameters on antenna performance. As can be observed from Figs. 4(a) and (b), parameters L_3 and W_3 for the meander line structure play an important role for controlling the resonance frequency needed in LTE 42/43 band (3.4–3.8 GHz). As noticed, the first and second resonances shift to lower frequencies, but the first one varies more than the second when L_3 is varied from 2 mm to 3 mm, and the value of W_3 increases from 1.5 mm to 1.9 mm. This means that the first resonance frequency at 3.75 GHz is

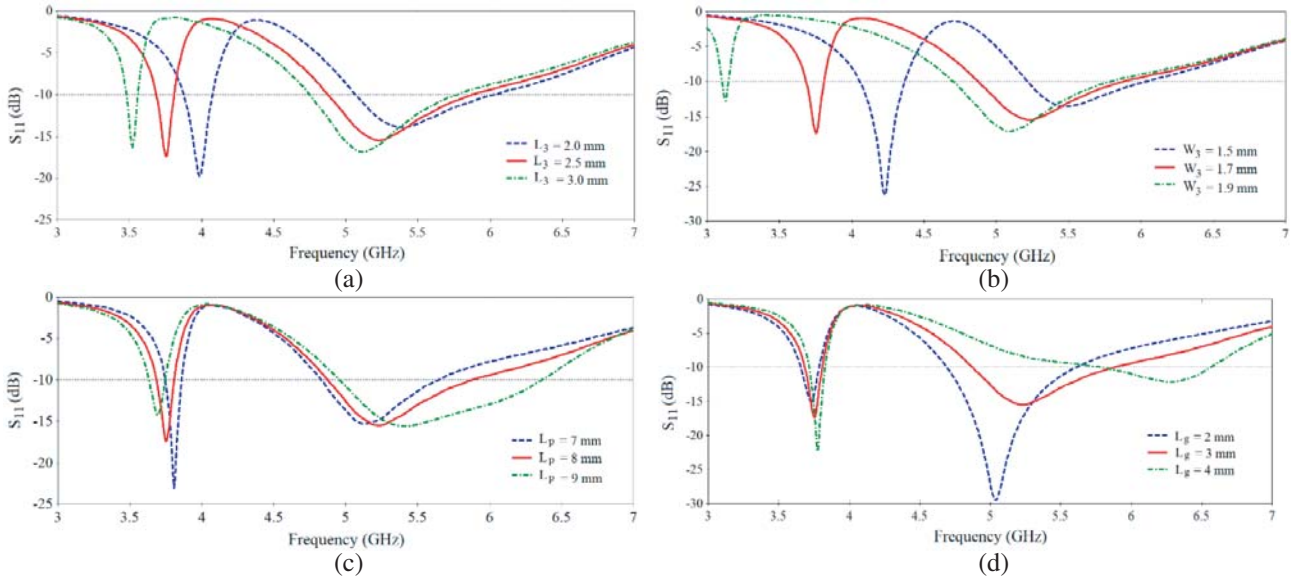

Figure 4. Simulated S_{11} of the single antenna as a function of (a) L_3, (b) W_3, (c) L_p, and (d) L_g.

generated by a fine-tuning approach and properly combining the meander strip line and spiral structure. Similarly, Figs. 4(c) and (d) indicate that the second resonance frequency at 5.2 GHz suitably used for LTE 46 band (5.150–5.925 GHz) is largely influenced by varying the spiral and ground lengths L_p and L_g, respectively. Therefore, it is worth mentioning here that the proposed antenna can cover the LTE 42/43 and 46 bands.

2.3. Performance of the Single Antenna

This section describes the performance parameters of the proposed antenna in terms of surface current distribution, gain, efficiency, and radiation patterns. The commercial software used to obtain these performance parameters is CST MWS.

2.3.1. Surface Current Distribution

Based on the reflection coefficient $|S_{11}|$ curve obtained previously, the single antenna element is operated at dual bands with resonant frequencies of 3.75 and 5.22 GHz. The obtained frequency ranges agree well with LTE 42/43/46 frequency bands. It is well known that each conductive strip element plays a key role in forming the antenna performance. To confirm this claim, the surface current distribution at the aforementioned two frequencies is plotted in Fig. 5. As observed, the surface current distribution is influenced by some elements of the spiral and meander line structures at these resonances, yielding two resonance frequencies in S_{11} curve of the antenna. Hence, each one of the branches in the radiating patch element is responsible for exciting resonance. The formula that governs the relation between excited resonance frequencies, antenna geometric parameters and physical characteristics is as follows [23]:

$$f_r = \frac{c}{2L_e}\sqrt{\frac{2}{\varepsilon_r + 1}} \tag{1}$$

where L_e is the total electric length of the structural antenna elements. Fig. 5 clarifies that properly tuning of spiral's dimensions and appropriate placement of meander line conductive element inside the spiral structure would yield the desired impedance bandwidth performance suitable for applicable frequency bands, LTE 43/46. Thus, more current flows for 3.75 GHz [Fig. 5(a)] at the edges of spiral and meander line segments whereas for 5.22 GHz [Fig. 5(b)] the current only spreads at the meander line element.

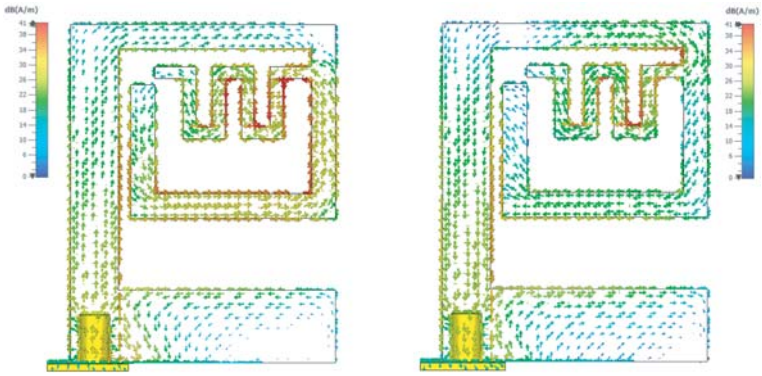

(a) (b)

Figure 5. Simulated surface current distributions at (a) 3.75 GHz and (b) 5.22 GHz.

2.3.2. Realized Gain and Efficiency

Figure 6 represents the realized gain and efficiency at the operating frequency bands LTE 43 and LTE 46 for the proposed antenna. More gain is obtained at higher frequency band (5.22 GHz) than lower frequency band (3.75 GHz). Fig. 6(b) clarifies that antenna efficiencies at the desired frequency bands (LTE 43 and LTE 46) are 77.5% and 91.3%, respectively.

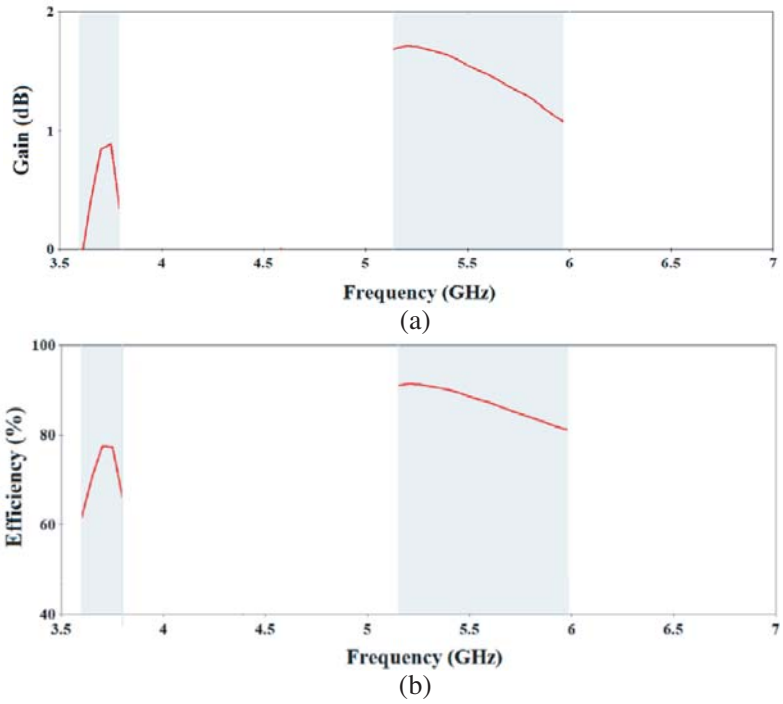

Figure 6. Simulated (a) realized gain and (b) efficiency for the proposed single antenna.

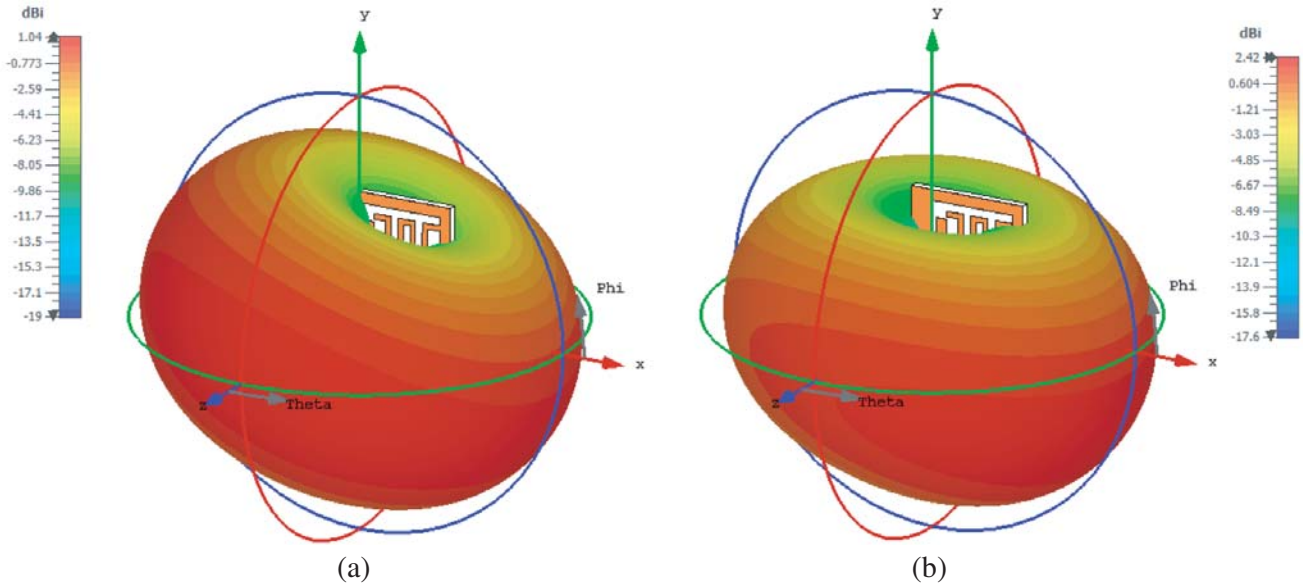

Figure 7. 3D radiation patterns of the proposed antenna at (a) 3.75 GHz and (b) 5.22 GHz.

2.3.3. Radiation Patterns

This section presents both the 3D and 2D radiation patterns at the resonance frequency in operating frequency bands (3.75 GHz and 5.22 GHz) for the proposed antenna. Fig. 7 shows the plot of 3D radiation patterns. It is seen from this figure that the antenna has an omnidirectional radiation patterns for each resonance frequency. Fig. 8 shows the 2D radiation pattern in the xz plane and xy plane at the two operating bands. As clear from the figure, the proposed antenna has a bidirectional radiation in the xy

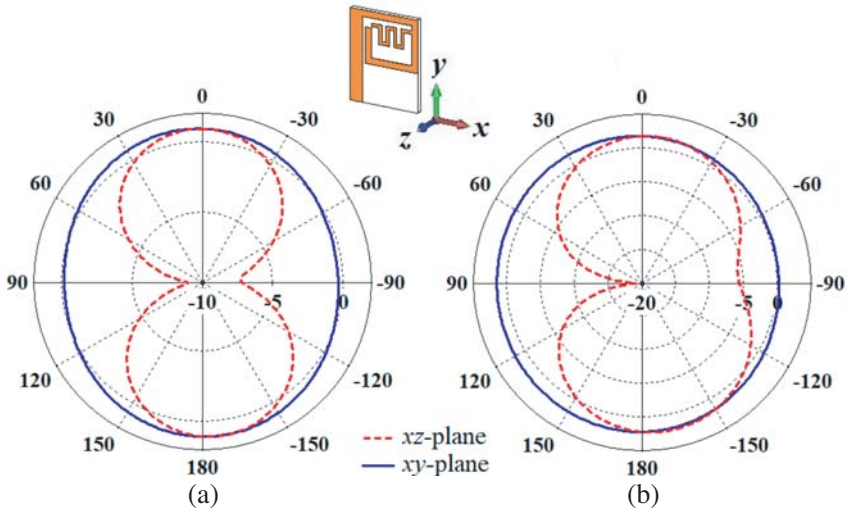

Figure 8. 2D radiation patterns for the proposed antenna at (a) 3.75 GHz and (b) 5.22 GHz.

or E plane for both the resonance frequencies (3.75 and 5.22 GHz), whereas the proposed antenna has nearly bidirectional radiation in the xz or H plane.

3. MIMO ANTENNA CONFIGURATIONS

The overall configurations of the proposed dual-band MIMO systems used in a handset terminal are shown in Fig. 9. In this figure, four types of MIMO antennas are depicted, orthogonal and parallel 4-, 6-, and 8-element MIMO systems besides a single-element antenna. As can be noticed in Figs. 9(a) and (b), 4 antenna elements, namely, antennas (Ants), 1–4 are disposed as orthogonal and parallel arrangements, respectively, along the 4 corners of the 0.8-mm FR4 substrate, which is used as a printed circuit board (PCB) in 6-in. smartphones with dimensions of 80 mm × 150 mm. Figs. 9(c) and (d) depict the geometry of the 6- and 8-element, namely, Ants 1–6 and 1–8, respectively, which constitute MIMO antenna array systems, printed on the front side of PCB (in orange), and ground plane (in gray) is printed on its back side. As can be observed in Fig. 9(c) for 6-element MIMO system, Ants 1, 3, 4,

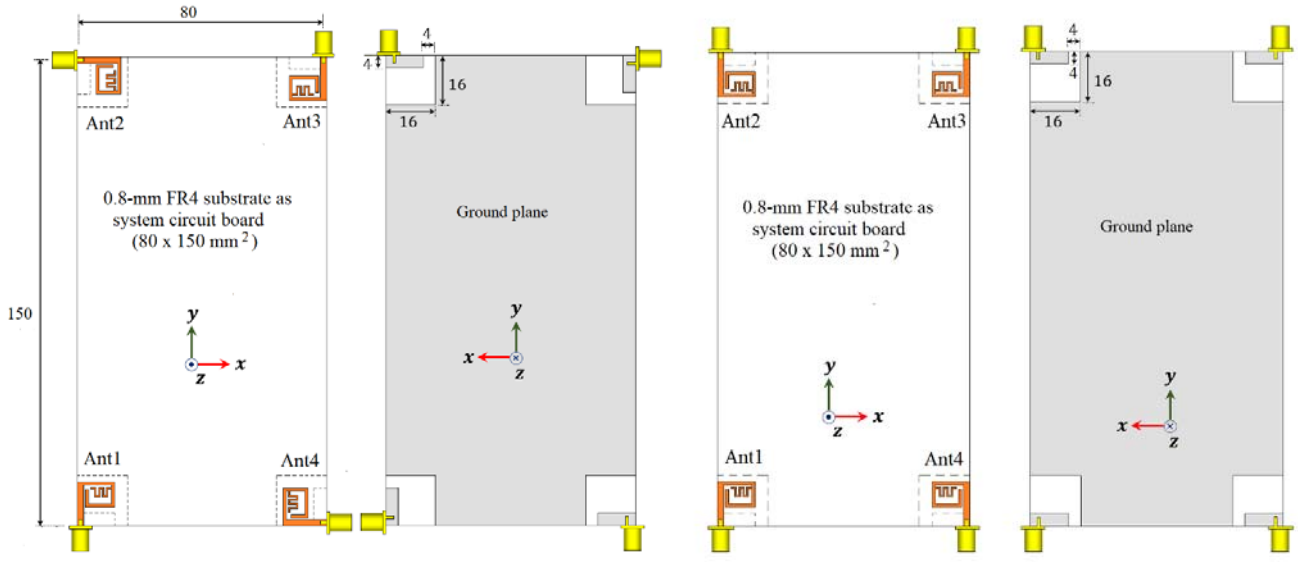

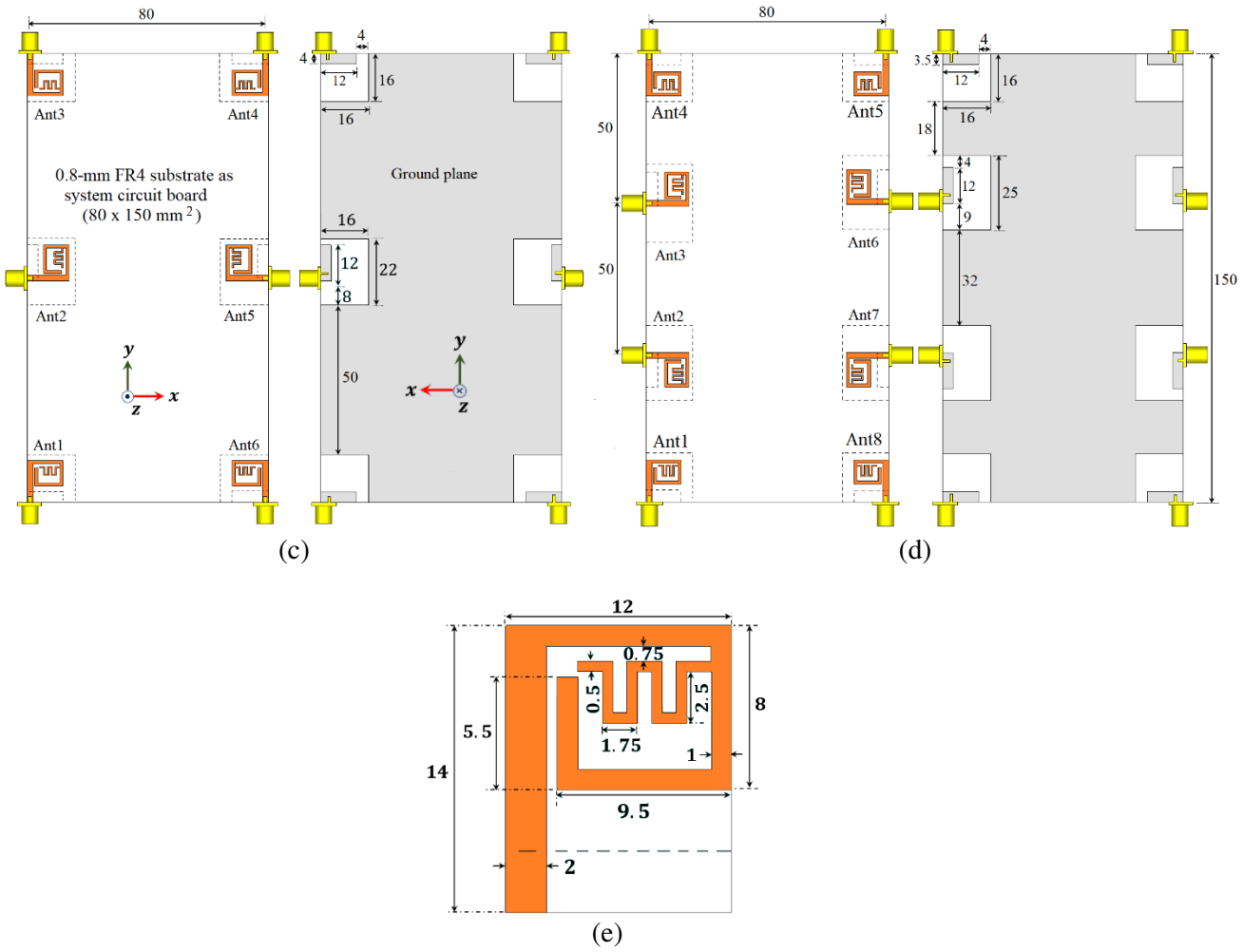

Figure 9. Configuration of the proposed (a) orthogonal four-element MIMO antenna, (b) parallel four-element MIMO antenna, (c) six-element MIMO antenna, (d) eight-element MIMO antenna, and (e) single-element antenna.

and 6 are vertically (y-axis) arranged at the four corners whereas Ants 2 and 5 are horizontally (x-axis) placed at the right and left sides of PCB. In the same manner, for 8-element MIMO antenna array, Fig. 7(d), Ants 1, 4, 5, and 8 (Ants 2, 3, 6, and 7) are horizontally (vertically) deployed along the corners (the middle) of the FR4 substrate.

The simulated S-parameters of the optimized proposed dual-band 4-, 6-, and 8-antenna MIMO systems are shown in Figs. 10 and 11. Due to the symmetric properties of the MIMO antenna systems, it is appropriate that only needful S-parameter curves for the adjacent antenna elements can be given. As noticed in Figs. 10(a) and (b), the 4-element MIMO systems for the orthogonal and parallel arrangements, respectively, cover both the lower and upper LTE bands (3.5 and 5.6 GHz). The reflection coefficient curves S_{11}, S_{22}, S_{33}, and S_{44} are less than -6 dB or VSWR < 3, and the isolations, S_{32} and S_{41}, are always better than -14 dB. The above results reveal that the proposed 2×2 MIMO antenna systems can ensure good isolation between the two neighboring antenna elements, and the desired dual-band frequency ranges have been achieved. Similarly, the reflection coefficient and isolation curves of Ants 1–6 and Ants 1–8 for 6- and 8-element MIMO systems, as shown in Figs. 11(a) and (b), respectively, indicate that a good performance in terms of S-parameters for the two MIMO systems has been obtained.

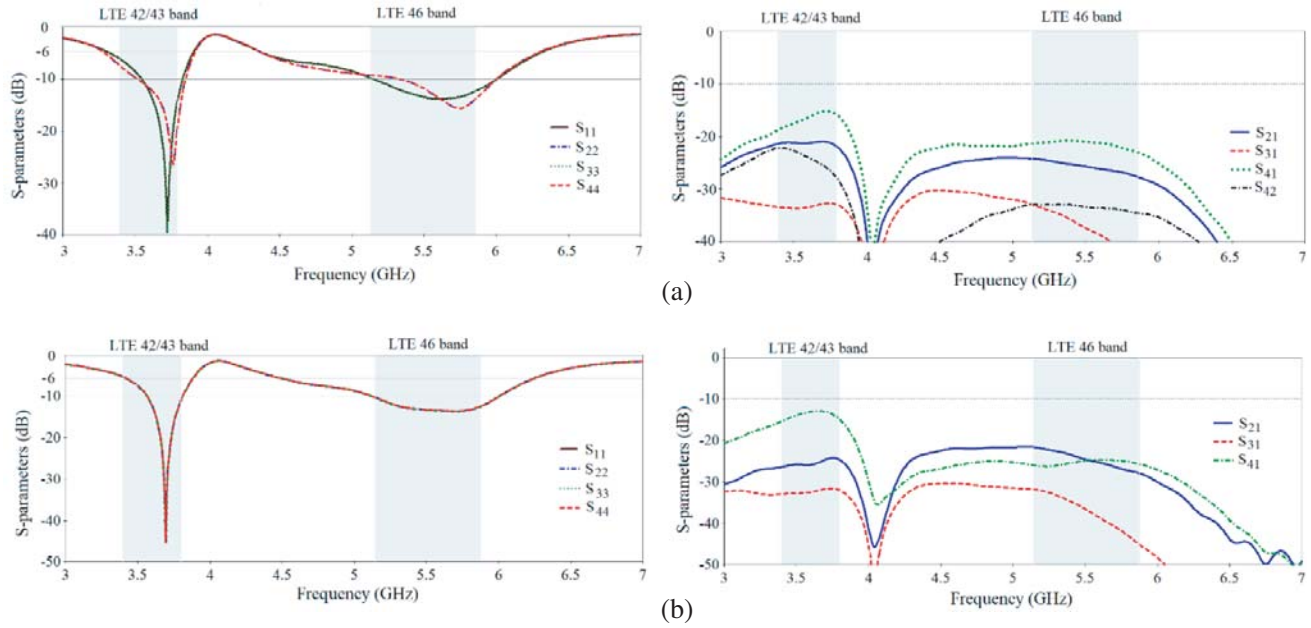

Figure 10. Simulated *S*-parameter of the proposed 4-element MIMO antenna system. (a) Orthogonally arranged. (b) Parallel arranged.

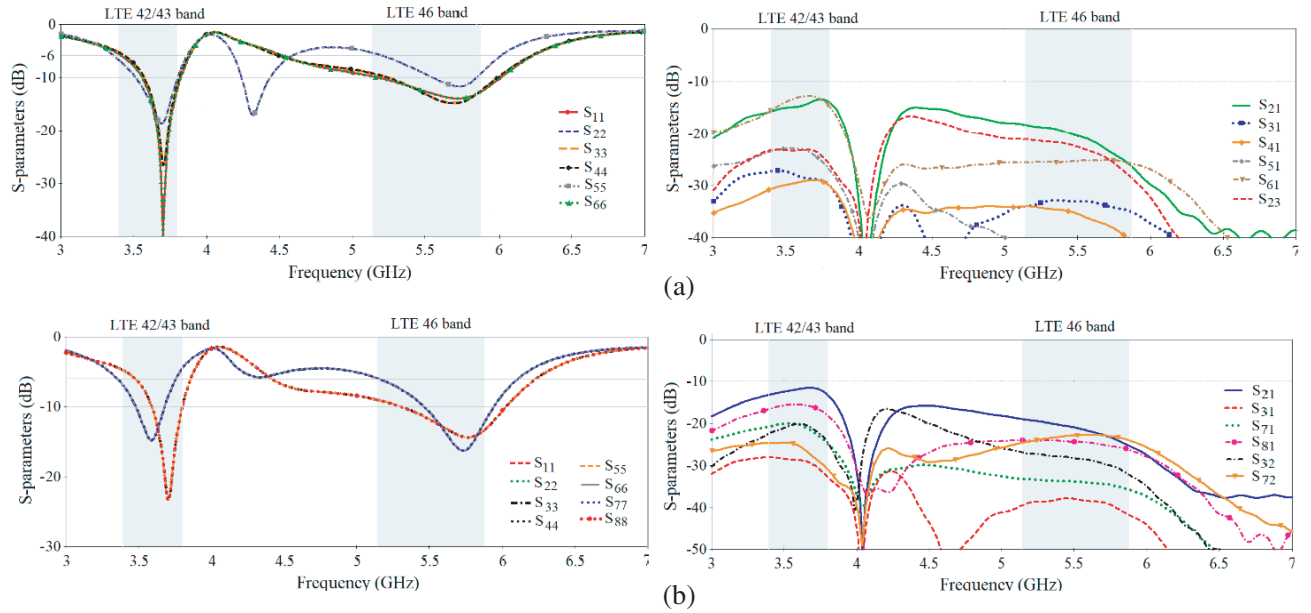

Figure 11. Simulated *S*-parameter of the proposed (a) 6-element and (b) 8-element MIMO antenna system.

4. THE PERFORMANCE EVALUATION OF MIMO ANTENNA SYSTEMS

In this section, the performance of designed MIMO antenna systems described previously (orthogonal and parallel 4-element, 6-, and 8-elements) are evaluated by necessary parameters such as far-field characteristic; gain, efficiency and radiation patterns; envelope correlation coefficient (ECC) and diversity gain (DG).

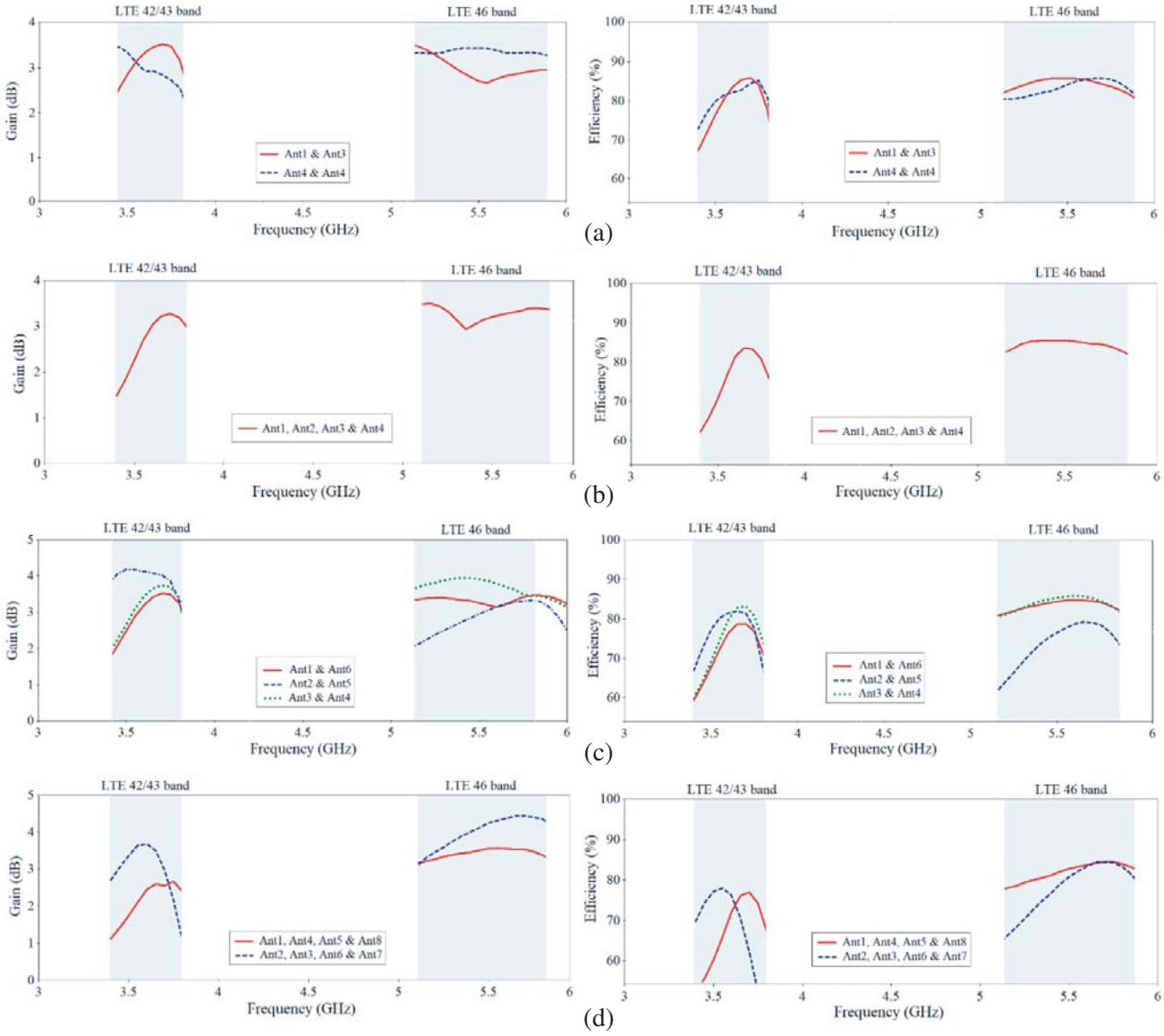

Figure 12. Simulated gain and efficiency for the proposed designs: (a) orthogonal 4-element, (b) parallel 4-element, (c) 6-element and (d) 8-element MIMO antenna systems.

4.1. The Realized Peak Gain, Efficiency, and Radiation Patterns

The simulated gain and efficiency for the four MIMO systems are shown in Fig. 12. It is observed from Figs. 12(a) and (b) that the gain and efficiency in the LTE 42/43 (LTE 46) band for the four antenna elements (Ant1 to Ant2) distributed in two arrangements, orthogonal and parallel, respectively, are greater than 2 dB and 60% (2.5 dB and 80%). Similarly, for the 6- and 8-element MIMO systems, Figs. 12(c) and (d), respectively, acceptable gain and efficiency are achieved for both the bands.

To maintain non-recurrence or repeated discussion, the 3D and 2D radiation patterns for only the 8-element MIMO system at 3.5 and 5.6 GHz are plotted in Figs. 13 and 14, respectively. It can be observed from Fig. 13 (for symmetry only Ant1 to Ant4 patterns are displayed) that Ant1, Ant2, Ant4, and Ant8 (at the four substrates' corners) have similar bi-directional radiation patterns (w.r.t. z-axis) with maximum values at the two sides of x-axis, and Ant3, Ant5, Ant6, and Ant7 (at the middle of PCB) are nearly bidirectional and radiate at one side of x-axis. Moreover, the 3D radiation patterns depicted in Fig. 13 indicate that each antenna radiates in a different direction from the other, which

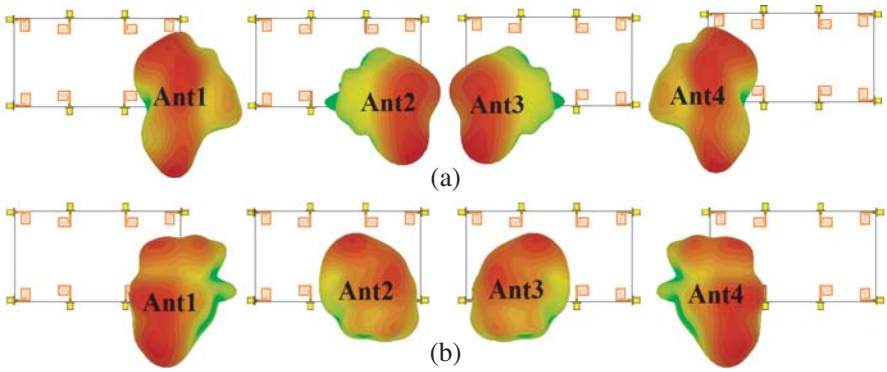

Figure 13. Simulated 3D antenna radiation patterns at (a) 3.5 GHz and (b) 5.6 GHz for the 8-antenna MIMO system.

demonstrates that the proposed MIMO system has the ability to radiate in all directions.

To further investigate the far-field performance of the 8-element MIMO system, the 2D radiation patterns (E- and H-plane) at the two resonance frequencies 3.5 and 5.6 GHz are displayed in Fig. 14. As observed, at 3.5 GHz [Fig. 14(a)] and at 5.6 GHz [Fig. 14(b)], Ant1, Ant2, Ant7, and Ant8 radiate at the top side in E-plane (xy-plane or $\phi = 0°$) and have maximum radiation at the left side of H-plane (yz-plane or $\theta = 90°$) whereas Ant3 to Ant6 radiate on the bottom side of E-plane, and their maximum radiation is at the right side of H-plane. Therefore, an approximately omnidirectional radiation in H-plane and bidirectional radiation in E-plane, for the two frequency bands (LTE 42/43) and (LTE 46), are achieved from each antenna (Ant1 to Ant8) of 8-antenna MIMO system.

4.1.1. Envelope Correlation Coefficient

One of the important parameters used for describing the degree of correlation between antenna elements of a MIMO system is Envelope Correlation Coefficient (ECC). Therefore, the ECC is widely adopted by researchers for estimating the diversity performance of the MIMO antenna systems, which are composed of radiating elements having the ability to simultaneously and independently transmit data streams. Hence, the radiators of antenna elements should have very weak ECC, less than 0.5, that is, good isolation must be provided by the MIMO antenna elements. For an N-port MIMO system, the correlation ρ_e between any two antenna elements (i and j) can be computed by the relation [24]

$$\rho_e(i,j,N) = \left| \frac{\sum_{n=1}^{N} S_{i,n}^{*} S_{n,j}}{\left| \prod_{k=i,j} \left(1 - \sum_{n=1}^{N} S_{k,n}^{*} S_{n,k} \right) \right|^{1/2}} \right|^2 \tag{2}$$

For instance, by substitution in Eq. (2), $N = 4$ and i or j takes the values of 1, 2, 3, or 4, one can obtain for example $\rho_e(1,2,4)$, that is ECC 12 for 4-element MIMO system as follows:

$$\rho_e(1,2,4) = \frac{\left| S_{11}^{*} S_{12} + S_{21}^{*} S_{22} + S_{13}^{*} S_{32} + S_{14}^{*} S_{42} \right|^2}{\left(1 - |S_{11}|^2 - |S_{21}|^2 - |S_{31}|^2 - |S_{41}|^2 \right) \left(1 - |S_{12}|^2 - |S_{22}|^2 - |S_{32}|^2 - |S_{42}|^2 \right)} \tag{3}$$

In a similar manner, it is easy to calculate the ECC for any value of a number of ports (N) and between antenna elements (i and j). By using Eq. (2), the simulated ECCs against frequency for the proposed MIMO antenna system ($N = 4$, 6, and 8) are plotted in Figs. 15(a)–(d). It can be observed from Fig. 15 that the ECCs throughout the frequency bands for the four MIMO systems are below 0.5, meaning good isolation between their antenna elements. Therefore, the proposed MIMO systems have an acceptable diversity performance making them suitable for using in portable mobile terminals.

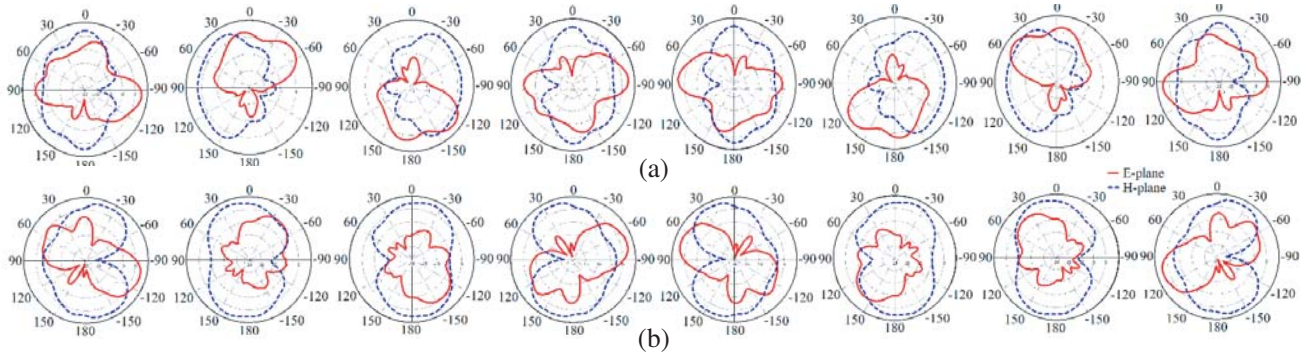

Figure 14. Simulated 2D antenna radiation patterns at (a) 3.5 GHz and (b) 5.6 GHz for the 8-antenna MIMO system, Ant1 (left) to Ant8 (right).

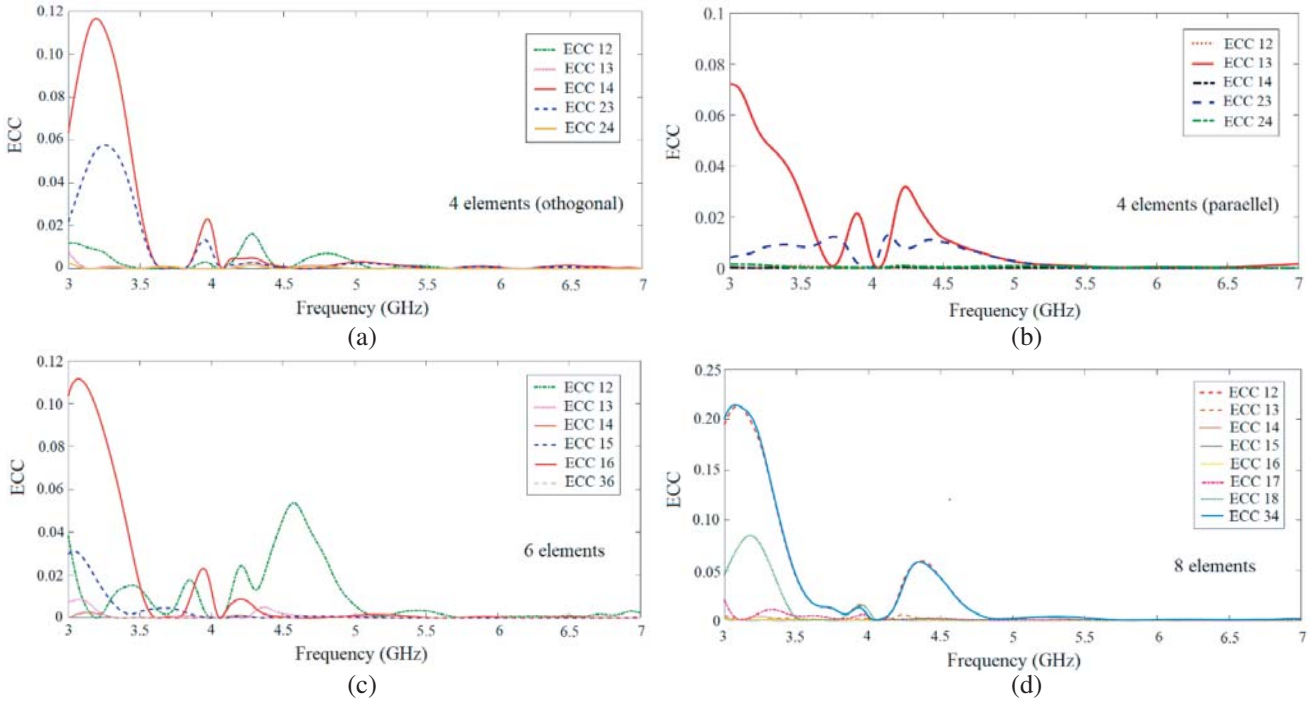

Figure 15. Simulated envelope correlation coefficient for the proposed designs: (a) orthogonal 4-element, (b) parallel 4-element, (c) 6-element and (d) 8-element MIMO antenna systems.

4.2. Diversity Gain

The diversity gain (DG) of a MIMO antenna system represents an important parameter considered in the use of different diversity approaches of MIMO antenna leading to increase in the signal to interference ratio [4] and can be computed by:

$$DG = 10\sqrt{1 - |\rho_e|} \tag{4}$$

It is clear from Eq. (4) that the diversity gain is mainly dependent on the correlation coefficient ρ_e, with maximum value in DG of 10 which is achieved for $\rho_e = 0$, and the better in DG comes from the lower value of ECC. Applying Eq. (4) for the four proposed MIMO systems that have the worst ECC curve is shown in Fig. 15, that is ECC 12, and one can plot DG (in dB) as a function of frequency as depicted in Fig. 16. It is observed from Fig. 16 that the diversity gain is more than 9.9 dB for the LTE 42/43 band (3.4–3.8 GHz) and nearly 10 dB for the LTE 46 band (5.150–5.925 GHz).

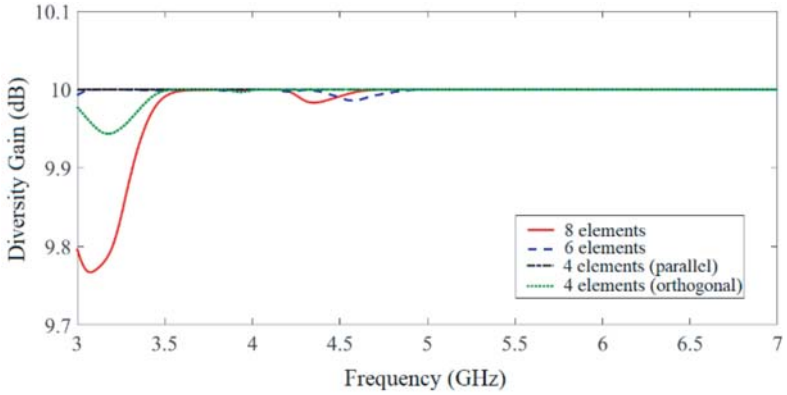

Figure 16. Simulated diversity gains for the proposed MIMO antenna systems.

5. THE MEASURED RESULTS OF SINGLE ELEMENT AND 8-ELEMENT MIMO SYSTEM

In order to verify the performance characteristics of the proposed single antenna element and eight-port MIMO system, which comprises antenna elements organized in a pattern of 2×4 cells, they are fabricated as shown in Figs. 17 and 18, respectively with overall dimensions $11 \times 14 \times 0.8\,\text{mm}^3$ and $150 \times 80 \times 0.8\,\text{mm}^3$, respectively. The prototypes verification is carried out by comparing their simulated and measured results. The magnitude (in dB) of the simulated and measured reflection coefficients S_{11} of the single element antenna are shown in Fig. 19. It can be noticed that the two results are fairly close to each other, thus validating both the design concept of proposed antenna and its implementation. Table 3 summarizes both the simulated and measured $-6\,\text{dB}$ and $-10\,\text{dB}$-S_{11} frequency bands (band 1 and band 2) for the single antenna. As observed from Fig. 19 and Table 3, these two bands satisfy the LTE 43 band (3.6–3.8 GHz) and LTE 46 band (5.150–5.925 GHz), respectively.

The measured and simulated S-parameters of the 8-element MIMO antenna system are given in Fig. 20. A close agreement between the measurement and simulation results is generally obtained, and some slight deviations between them are due to inaccuracy in the fabrication process, SMA soldering, or uncertainty in the available substrate properties such as height and dielectric constant. To be specific, as observed from Fig. 20(a), both the y- and x-axis polarized antennas (Ant1, Ant4, Ant5, and Ant8) and (Ant2, Ant3, An6, and Ant7), respectively, have good measured reflection coefficients better than $-6\,\text{dB}$ for LTE 46 and 43 bands (5.150–5.925 GHz) and (3.6–3.8 GHz), respectively and somewhat can

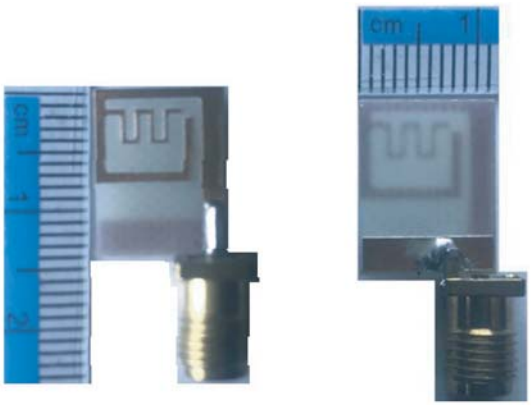

(a) (b)

Figure 17. Picture of the fabricated proposed single antenna element, (a) top layer and (b) bottom layer.

(a) (b)

Figure 18. Pictures of the fabricated proposed 8-element MIMO antenna system, (a) top layer and (b) bottom layer.

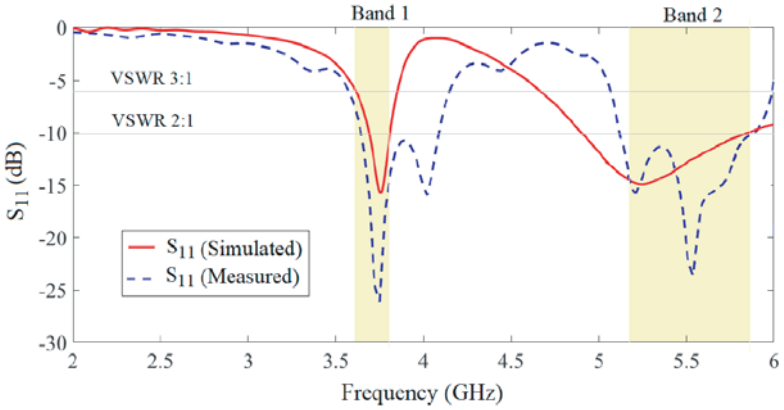

Figure 19. Simulated and measured reflection coefficient of the single antenna.

Table 3. The simulated and measured bands (in GHz) of the proposed single antenna.

Frequency bands	Band 1				Band 2			
	f_L		f_H		f_L		f_H	
Criterion	**−6 dB**	**−10 dB**	**−6 dB**	**−10 dB**	**−6 dB**	**−10 dB**	**−6 dB**	**−10 dB**
Simulated	3.61	3.68	3.84	3.80	4.65	4.87	> 6.00	5.87
Measured	3.58	3.64	4.15	4.08	5.10	5.05	5.98	5.88

also cover LTE 42 band (3.4–3.6 GHz). Thus, the general requirement for handset antenna designs is achieved from the proposed MIMO antenna system. As noticed in Fig. 20(b), for brevity and because of the symmetry disposition of the 8-antenna array, only maximally 4 curves are plotted for the simulated and measured transmission coefficients of S_{21}, S_{32}, S_{81}, and S_{72}. From the figure, the maximum couplings between any two neighboring antennas are all lower than −16.5 dB over the entire working frequency range (3.0–6.0 GHz). Therefore, the antennas within the MIMO system have good mutual couplings thanks to their compact size and proper arrangement.

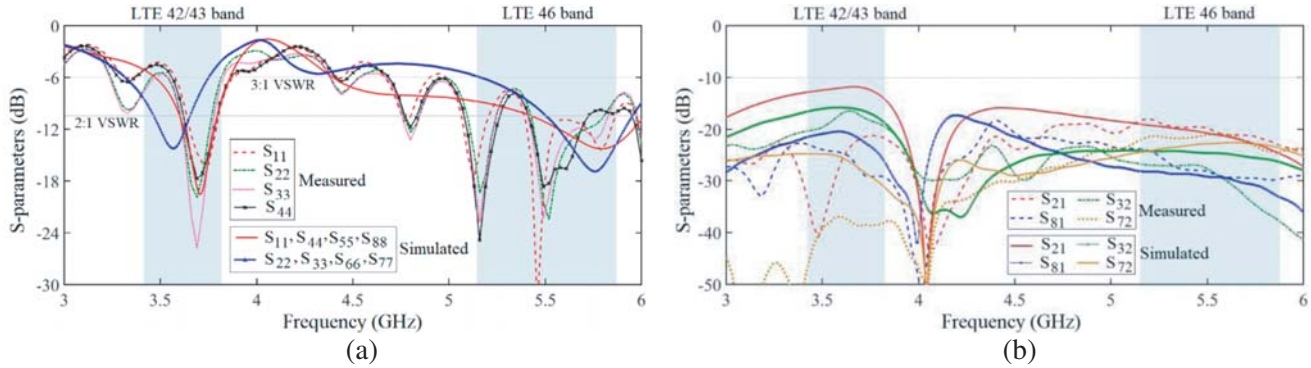

Figure 20. Simulated and measured *S*-parameters of the 8-element MIMO antenna system. (a) Reflection coefficients and (b) transmission coefficients.

Table 4 summarizes the performance of proposed MIMO antenna array and that of the previous published ones. It is clear that the proposed 8-antenna MIMO array, compared with the other, is able to operate within both LTE band 43 and LTE band 46. Moreover, the MIMO antenna system has ECC less than 0.05. Furthermore, an accepted efficiency is achieved by the proposed antenna at the two bands. Therefore, the proposed MIMO antenna can be used for 5G smartphone applications.

Table 4. Performance comparison between the proposed MIMO antenna array and reported ones.

Ref.	MIMO order	Ground size (mm^2)	Bandwidth (GHz)	Efficiency (%)	ECC (dB)
[5]	10	150 × 80	3.4–3.8 5.150–5.925 (−6 dB)	42–65 (low band) 62–82 (high band)	< 0.15
[15]	8	150 × 75	3.4–3.8 (−6 dB)	60	< 0.15
[16]	8	150 × 75	3.4–3.8 (−6 dB)	70	< 0.01
[17]	8	150 × 80	3.4–3.6 (−10 dB)	62–76	< 0.05
[18]	8	140 × 70	3.4–3.6 5.15–5.925 (−10 dB)	51–59 (low band) 62–80 (high band)	< 0.1
[19]	19	150 × 80	3.4–3.8 5.150–5.925 (−6 dB)	55.5–69.1 (low band) 48.9-62.8 (high band)	< 0.1
proposed	8	150 × 80	3.54–4.16 5.10–5.98 (−6 dB)	52.2–74.3 (low band) 65.4–82.2 (high band)	< 0.05

6. CONCLUSION

A new design approach for dual-band 4-, 6, and 8-element MIMO antenna systems for 5G operation in the smartphone has been reported in this paper. Because of using compact antenna elements arranged in orthogonal and horizontal patterns along the two side edges of the system board of a smartphone, good isolation can be obtained. The improved results, such as high isolation, good radiation characteristic, and other MIMO performance, can guarantee that the proposed antenna arrays will be preferred for the 5G smartphone applications, and they are especially useful for mobiles having large size display and multiband operation. Moreover, the proposed MIMO antenna systems have good impedance matching (reflection coefficients of better than −6 dB) covering LTE 42/43 band (3.4–3.8 GHz) and LTE 46 band (5.150–5.925 GHz) with better isolation (transmission coefficients of better than 10 dB), low envelope correlation coefficient (ECC < 0.1), and acceptable antenna efficiency ($> 70\%$ and 80%) for each antenna element at the low and high bands, respectively.

ACKNOWLEDGMENT

The authors would like to thank Dr. Ghassan N. Jawad from the University of Baghdad for providing the measurement results

REFERENCES

1. Andrews, J. G., S. Buzzi, W. Choi, S. V. Hanly, A. Lozano, A. C. K. Soong, and J. C. Zhang, "What will 5G be?" *IEEE J. Sel. Areas Commun.*, Vol. 32, No. 6, 1065–1082, Jun. 2014.
2. Ren, Z. and A. Zhao, "Dual-band MIMO antenna with compact self-decoupled antenna pairs for 5G mobile applications," *IEEE Access*, Vol. 7, 82288–82296, 2019.
3. Varzakas, P., "Average channel capacity for rayleigh fading spread spectrum MIMO systems," *International Journal of Communication Systems*, Vol. 19, No. 10, 1081–1087, 2006.
4. Sharma, M. K., M. Kumar, J. P. Saini, and S. P. Singh, "Computationally optimized MIMO antenna with improved isolation and extended bandwidth for UWB applications," *Arabian Journal for Science and Engineering*, 1–11, May 2019.
5. Li, Y., C.-Y.-D. Sim, Y. Luo, and G. Yang, "Multiband 10-antenna array for sub-6 GHz MIMO applications in 5-G smartphones," *IEEE Access*, Vol. 6, 28041–28053, 2018.
6. Zhao, A. and Z. Ren, "Multiple-input and multiple-output antenna system with self-isolated antenna element for fifth-generation mobile terminals," *Microwave and Optical Technology Letters*, Vol. 61, No. 1, 20–27, 2019.
7. Roy, S., S. Ghosh, and U. Chakarborty, "Compact dual wide-band four/eight elements MIMO antenna for WLAN applications," *International Journal of RF and Microwave Computer-Aided Engineering*, e21749, 2019.
8. Qin, Z., W. Geyi, M. Zhang, and J. Wang, "Printed eight-element MIMO system for compact and thin 5G mobile handset," *Electronics Letters*, Vol. 52, No. 6, 416–418, 2016.
9. Barani, I. R. R., K.-L. Wong, Y.-X. Zhang, and W.-Y. Li, "Low-profile wideband conjoined open-slot antennas fed by grounded coplanar waveguides for 4 W 4 5G MIMO operation," *IEEE Transactions on Antennas and Propagation*, 2019.
10. Wong, K.-L., Y.-H. Chen, and W.-Y. Li, "Decoupled compact ultra-wideband MIMO antennas covering 3300 $\sim$ 6000 MHz for the fifth-generation mobile and 5 GHz-WLAN operations in the future smartphone," *Microwave and Optical Technology Letters*, Vol. 60, No. 10, 2345–2351, 2018.
11. Huang, C., Y.-C. Jiao, and Z.-B. Weng, "Novel compact CRLH-TL-based tri-band MIMO antenna element for the 5G mobile handsets," *Microwave and Optical Technology Letters*, Vol. 60, No. 10, 2559–2564, 2018.
12. Alsaif, H., M. Usman, M. T. Chughtai, and J. Nasir, "Cross polarized 2×2 UWB-MIMO antenna system for 5G wireless applications," *Progress In Electromagnetics Research M*, Vol. 76, 157–166, 2018.

13. Idrees Magray, M., G. S. Karthikeya, K. Muzaffar, and S. K. Koul, "Corner bent integrated design of 4G LTE and mmWave 5G antennas for mobile terminals," *Progress In Electromagnetics Research M*, Vol. 84, 167–175, 2019.
14. Hussain, R., A. T. Alreshaid, S. K. Podilchak, and M. S. Sharawi, "Compact 4G MIMO antenna integrated with a 5G array for current and future mobile handsets," *IET Microw. Antennas Propag.*, Vol. 11, No. 2, 271–279, 2017.
15. Parchin, N. O., Y. I. A. Al-Yasir, A. H. Ali, I. Elfergani, J. M. Noras, J. Rodriguez, and R. A. Abd-Alhameed, "Eight-element dual-polarized MIMO slot antenna system for 5G smartphone applications," *IEEE Access*, Vol. 7, 15612–15622, 2019.
16. Parchin, N. O., H. Jahanbakhsh, M. Alibakhshikenari, Y. Ojaroudi, Y. I. Al-Yasir, R. A. Abd-Alhameed, and E. Limiti, "Mobile-phone antenna array with diamond-ring slot elements for 5G massive MIMO Systems," *Electronics*, Vol. 8, No. 5, 1–17, 2019.
17. Li, Y., Y. Luo, and G. Yang, "High-isolation 3.5 GHz eight-antenna MIMO array using balanced open-slot antenna element for 5G smartphones," *IEEE Transactions on Antennas and Propagation*, Vol. 67, No. 6, 3820–3830, 2019.
18. Li, J., X. Zhang, Z. Wang, X. Chen, J. Chen, Y. Li, and A. Zhang, "Dual-band eight-antenna array design for MIMO applications in 5G mobile terminals," *IEEE Access*, Vol. 7, 71636–71644, 2019.
19. Li, Y. and G. Yang, "Dual-mode and triple-band 10-antenna handset array and its multiple-input multiple-output performance evaluation in 5G," *International Journal of RF and Microwave Computer-Aided Engineering*, Vol. 29, No. 2, e21538, 2019.
20. Pedram, K., M. Naderi, F. S. Jafari, and F. B. Zarrabi, "Compact quad-band second harmonic antenna based on metamaterial DRA load," *Microwave and Optical Technology Letters*, Vol. 61, No. 8, 1938–1944, 2019.
21. Jabar, A. A. S. A. and D. K. Naji, "Design of miniaturized quad-band dual-arm spiral patch antenna for RFID, WLAN and WiMAX applications," *Progress In Electromagnetics Research C*, Vol. 91, 97–113, 2019.
22. Jabar, A. A. S. A. and D. K. Naji, "Optimization design methodology of miniaturized five-band antenna for RFID, GSM, and WiMAX applications," *Progress In Electromagnetics Research B*, Vol. 83, 177–201, 2019.
23. Balanis, C. A., *Antenna Theory: Analysis and Design*, 4th Edition, John Wiley & Sons, 2016.
24. Naji, D. K., "Design of a compact orthogonal broadband printed MIMO antennas for 5-GHz ISM band operation," *Progress In Electromagnetics Research B*, Vol. 64, 47–62, 2015.